Cannabinoid type 1 receptor-containing axons innervate NPY/AgRP neurons in the mouse arcuate nucleus

Yury M. Morozov, Marco Koch, Pasko Rakic, Tamas L. Horvath

Angaben zur Veröffentlichung / Publication details:

Morozov, Yury M., Marco Koch, Pasko Rakic, and Tamas L. Horvath. 2017. "Cannabinoid type 1 receptor-containing axons innervate NPY/AgRP neurons in the mouse arcuate nucleus." *Molecular Metabolism* 6 (4): 374–81. https://doi.org/10.1016/j.molmet.2017.01.004.

Brief Communication

MOLECULAR METABOLISM

Cannabinoid type 1 receptor-containing axons innervate NPY/AgRP neurons in the mouse arcuate nucleus

Yury M. Morozov [1,2,**], **Marco Koch** [3,4], **Pasko Rakic** [1,2], **Tamas L. Horvath** [3,*]

ABSTRACT

Objectives: Phytocannabinoids, such as THC and endocannabinoids, are well known to promote feeding behavior and to control energy metabolism through cannabinoid type 1 receptors (CB_1R). However, the underlying mechanisms are not fully understood. Generally, cannabinoid-conducted retrograde dis-inhibition of hunger-promoting neurons has been suggested to promote food intake, but so far it has not been demonstrated due to technical limitations.

Methods: We applied immunohistochemical labeling of CB_1R for light microscopy and electron microscopy combined with three-dimensional reconstruction from serial sections in CB_1R-expressing and CB_1R-null mice, which served as a negative control. Hunger-promoting neurons expressing Agouti-related protein and neuropeptide Y (AgRP/NPY) in the hypothalamic arcuate nucleus were identified in NPY-GFP and NPY-hrGFP mice.

Results: Using three-dimensional reconstruction from serial sections we demonstrated numerous discontinuous segments of anti-CB_1R labeling in the synaptic boutons and axonal shafts in the arcuate nucleus. We observed CB_1R in the symmetric, presumed GABAergic, synaptic boutons innervating AgRP/NPY neurons. We also detected CB_1R-containing axons producing symmetric and asymmetric synapses onto AgRP/NPY-negative neurons. Furthermore, we identified CB_1R in close apposition to the endocannabinoid (2-arachidonoylglycerol)-synthesizing enzyme diacylglycerol lipase-alpha at AgRP/NPY neurons.

Conclusions: Our immunohistochemical and ultrastructural study demonstrates the morphological substrate for cannabinoid-conducted feeding behavior via retrograde dis-inhibition of hunger-promoting AgRP/NPY neurons.

Keywords Hypothalamus; Arcuate nucleus; Agouti-related protein; Neuropeptide Y; Electron microscopy; 3D reconstruction

1. INTRODUCTION

Regulation of food intake and energy consumption is a complex system that includes multiple regulations of brain and peripheral organs [1–4]. As a group of lipid messengers, endocannabinoids (eCBs) have the capability to induce synaptic plasticity by retrograde modulation of glutamatergic and GABAergic neurotransmission in various brain areas as well as represent important metabolic signaling molecules in peripheral organs [1,5,6]. Indeed, cannabinoid type 1 receptors (CB_1R) are well known to mediate the effects of cannabinoids on energy metabolism [7–10]. Novel data indicate that the anorexigenic proopiomelanocortin (POMC) neurons reverse their function in the presence of cannabinoids [11,12]. However, the cellular and molecular mechanisms behind hypothalamic CB_1R activation in order to regulate energy expenditure and feeding behavior are still not fully understood [10,13]. POMC neurons affect whole body energy metabolism in tandem with neurons in the hypothalamic arcuate nucleus (ARC) that co-express Agouti-related protein (AgRP) and neuropeptide Y (NPY; [14]). At times of negative energy balance, AgRP/NPY neurons are directly activated by the appetite-inducing hormone ghrelin and by increased levels of free fatty acids that are utilized in these neurons via beta-oxidation [15]. Upon activation, AgRP/NPY neurons release neuropeptides as well as GABA to control behavior, in part by inhibiting POMC neurons in the ARC [16]. In parallel to the feeding-promoting hormone ghrelin, distinct eCBs such as 2-arachodonoylglycerol (2-AG) are up regulated in the hypothalamus during fasting, whereas satiety-promoting hormones such as leptin acutely reduce hypothalamic 2-AG levels [7,17,18]. This prandial state-dependent fluctuation of the retrograde messenger 2-AG indicates that eCBs might be involved in regulation of hypothalamic AgRP/NPY neurons. Previous

[1]Department of Neuroscience, Yale University School of Medicine, 06520 New Haven, CT, USA [2]Kavli Institute for Neuroscience, Yale University School of Medicine, 06520 New Haven, CT, USA [3]Program in Integrative Cell Signaling and Neurobiology of Metabolism, Section of Comparative Medicine, Yale University School of Medicine, 06520 New Haven, CT, USA [4]Institute of Anatomy, University of Leipzig, 04103 Leipzig, Germany

*Corresponding author. Program in Integrative Cell Signaling and Neurobiology of Metabolism, Section of Comparative Medicine, Yale University School of Medicine, 06520-8016 New Haven, CT, USA. E-mail: tamas.horvath@yale.edu (T.L. Horvath).

**Corresponding author. Department of Neuroscience, Yale University School of Medicine, 06520 New Haven, CT, USA. E-mail: yury.morozov@yale.edu (Y.M. Morozov).

Received December 6, 2016 • Revision received January 4, 2017 • Accepted January 9, 2017 • Available online 27 January 2017

http://dx.doi.org/10.1016/j.molmet.2017.01.004

studies demonstrated moderate amounts of radioactive CB_1R ligand binding as well as CB_1R mRNA in hypothalamic nuclei [13,19–21]. However, AgRP/NPY neurons do not contain CB_1R mRNA and it is thus unlikely that cannabinoids directly affect the output synapses of AgRP/NPY neurons [19]. Nevertheless, retrograde eCB modification of presynaptic CB_1R on glutamatergic or GABAergic axon terminals innervating AGRP/NPY neurons was suggested as a putative mechanism of eCB-dependent control of AgRP/NPY activity, but CB_1R immunolabeling remained uncertain in the ARC [6,22–24]. This inspired our immunohistochemical investigation of eCB signaling in the ARC. Here, we used transgenic mouse models and methods of electron microscopy combined with three-dimensional (3D) reconstruction from serial sections to evaluate the morphological substrate of presynaptic CB_1R-dependent control of AgRP/NPY neurons in the ARC.

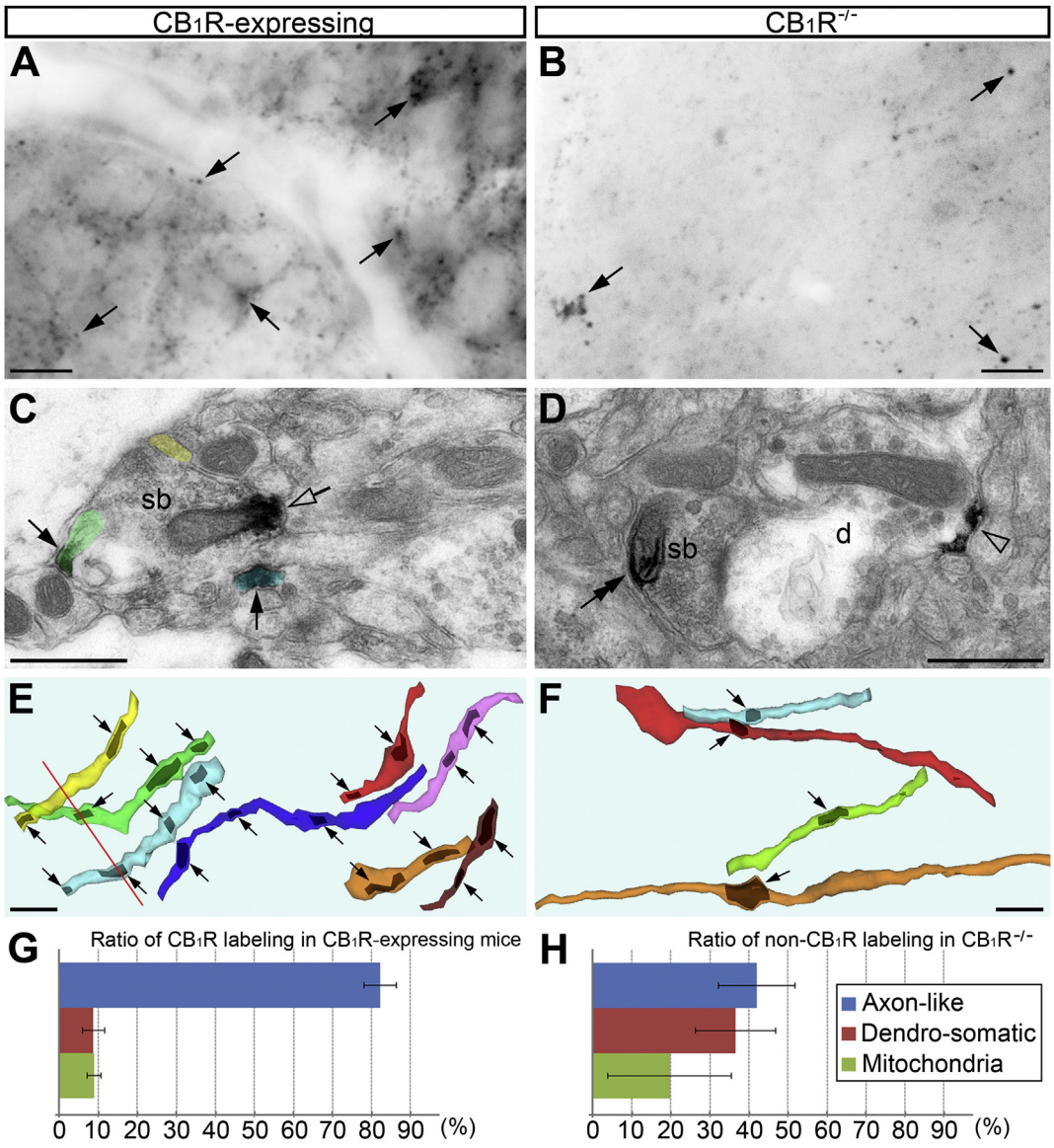

Figure 1: Light and electron microscopy of the hypothalamus from CB_1R-expressing mice and $CB_1R^{-/-}$ littermates immunolabeled with anti-CB_1R serum. (**A and B**) Representative light micrographs of ARC from $CB_1R^{+/-}$ (**A**) and $CB_1R^{-/-}$ mice (**B**). Equal conditions of the tissue and micrograph preparation were applied. The micrographs show numerous immunopositive particles (arrows) in $CB_1R^{+/-}$ and similar but relatively rare staining in $CB_1R^{-/-}$. (**C and D**) Electron microscopy analysis shows that, in the $CB_1R^{+/-}$, numerous immunolabeling depositions are located in thin axon-like processes (arrows); atypical staining is also present. For example, it is unclear whether the DAB-Ni deposition between the axonal cell membrane and mitochondria (empty arrow) results from selective labeling of membranous CB_1R or cross reactivity with mitochondrial stomatin-like protein 2 [27–29]. Electron micrograph from $CB_1R^{-/-}$ shows non-selective DAB-Ni deposition in a dendrite (empty arrowhead) and mitochondrial labeling characteristic for stomatin-like protein 2 (double arrow). (**E and F**) 3D reconstructions from serial ultrathin sections of arbitrarily chosen axon-like processes (each depicted with different colors in semitransparent mode) that contain DAB-Ni depositions (depicted black; arrows). The processes in $CB_1R^{+/-}$ contain numerous immunopositive fragments, whereas axon-like processes contain single spots of DAB-Ni deposition in $CB_1R^{-/-}$. Red line in E indicates positioning of the profiles shown in the electron micrograph in C where they are highlighted with the same semitransparent colors, respectively. (**G and H**) Electron microscopy quantifications of the anti-CB_1R immunolabeling in identified cell segments and organelles in ARC of the CB_1R-expressing ($CB_1R^{+/+}$ and $CB_1R^{+/-}$, pooled) and $CB_1R^{-/-}$ mice. Notice that anti-CB_1R immunolabeling predominates in the axon-like processes in the CB_1R-expressing animals (**G**); this is not encountered in $CB_1R^{-/-}$ mice (**H**). This confirms presence of CB_1R in the axons while dendro-somatic and mitochondrial CB_1R locations are enigmatic. Averages of the measurements from 4 animals in each group ±SD are indicated. Abbreviations: d, dendrite; sb, synaptic bouton. (Scale bars in **A and B** = 10 μm; in **C–F** = 0.5 μm).

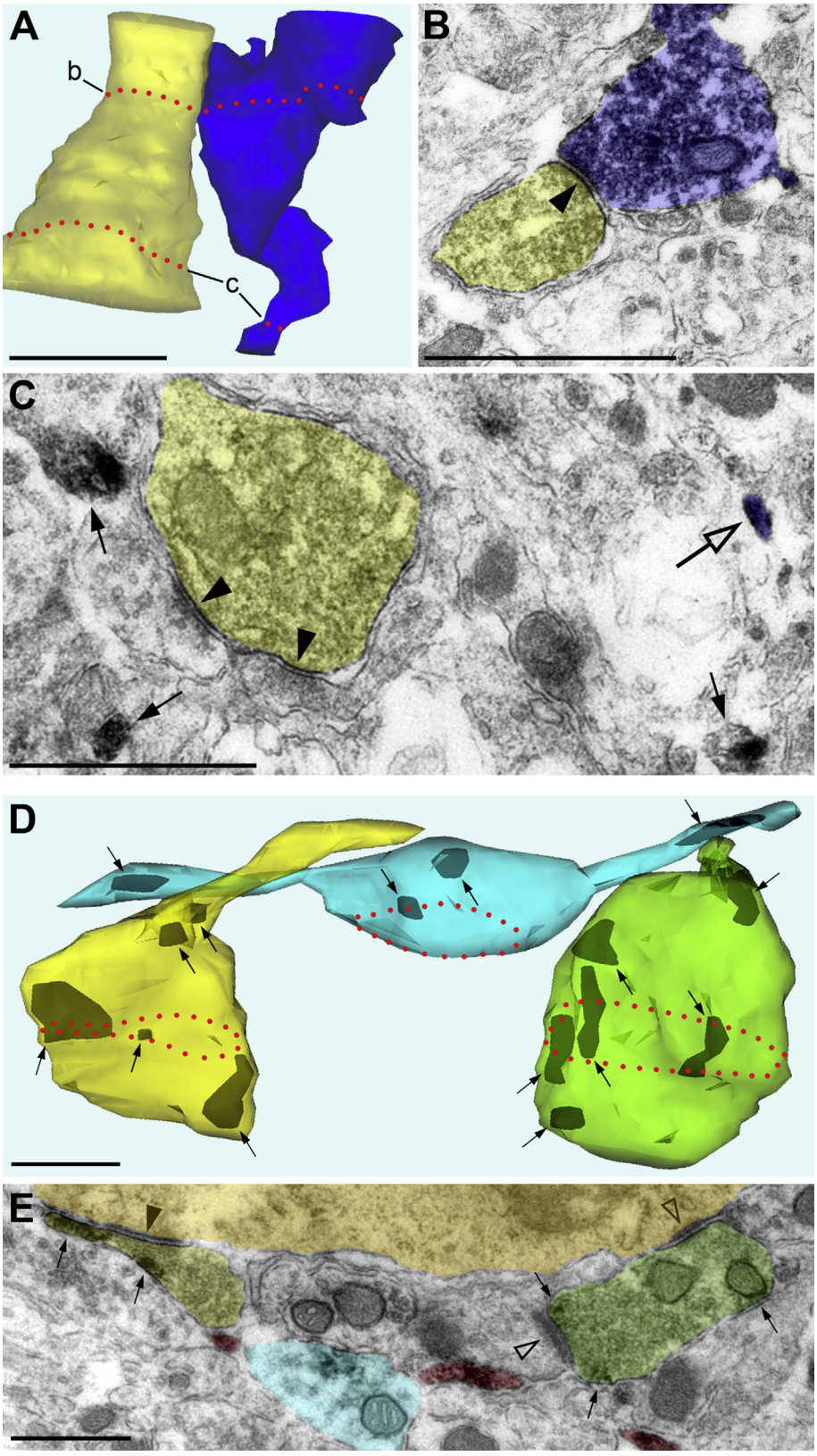

Figure 2: CB_1R in synaptic boutons innervating AgRP/NPY-positive and -negative neurons in the ARC. (**A**–**C**) In 3D reconstruction, NPY-GFP-positive dendritic shaft (yellow) contacts with CB_1R-positive axon (blue). Positions of profiles shown in electron micrographs (**B and C**) are indicated with red dotted lines b and c, respectively. (**B**) NPY-GFP-positive dendrite identified with diffuse DAB deposition (highlighted semitransparent yellow) produces symmetric synapse (arrowhead) with CB_1R-positive synaptic bouton (semitransparent blue) that is identified with intense black DAB-Ni staining. (**C**) The NPY-GFP-positive dendrite is also innervated by two symmetric synapses (arrowheads) from CB_1R-negative axons. Profile of axonal shaft of the reconstructed CB_1R-positive axon is indicated with empty arrow. Profiles of other CB_1R-positive axons not shown in the 3D

2. METHODS

2.1. Animal maintenance

Mice were maintained with water and food freely available and housed on a 12 h light/12 h dark cycle. All mice were aged between 12 and 16 weeks at the time of killing. Procedures were approved by the Institutional Animal Care and Use Committee of Yale University.

2.2. Transgenic animals

CB_1R-null ($CB1R^{-/-}$) mice were on a C57/BL6 background [25]. NPY-GFP (B6.Cg-Tg(Npy-MAPT/Sapphire)1Rck/J, stock no 008321, The Jackson Laboratories, Bar Harbor, ME USA) and NPY-hrGFP (B6.FVB-Tg(Npy-hrGFP)1Lowl/J, stock no 006417, The Jackson Laboratories) mice were used for identification of AgRP/NPY neurons in the ARC. Both lines were maintained on a C57/BL6 background.

2.3. Immunohistochemistry for electron and light microscopy

For correlative light/electron microscopy, $CB_1R^{+/+}$, $CB1R^{+/-}$, $CB1R^{-/-}$ and NPY-GFP mice were perfused transcardially with a fixative containing 4% paraformaldehyde, 0.2% picric acid, and 0.2% glutaraldehyde in 0.1 M PB. The brains were removed and immersed overnight in the same fixative. Coronal brain sections (of 50 μm thickness) were cut with a vibratome. About half of the brain sections were immersed in 0.5% H_2O_2 for 30 min to block tissue peroxidase, whereas the remaining specimens were used for immunohistochemistry omitting this step. No difference in the immunolabeling was observed between these sections. For single immunolabeling, the sections were incubated with polyclonal sera against CB_1R raised in guinea pig (1:1000; CB1-GP-Af530; Frontier Institute, Ishikari, Hokkaido, Japan), then, with biotinylated anti-guinea pig IgGs (1:300; Jackson Immunoresearch, West Grove, PA, USA) and the Elite ABC kit (Vector Laboratories, Burlingame, CA, USA) with Ni-intensified 3,3′-diaminobenzidine-4HCl (DAB-Ni) as a chromogen. For CB_1R/GFAP and CB_1R/NPY-GFP double labeling, the sections were first immunolabeled for CB_1R as above with DAB-Ni as a chromogen that produces intensive black staining; then, the sections were incubated with made-in-rat anti-GFAP (1:6000; Invitrogen, Eugene, OR, USA) or made-in-chicken anti-GFP (1:2000; Thermo Fisher Scientific, Rockford, IL, USA) sera. Thereafter, corresponding biotinylated anti-rat or anti-chicken IgGs (1:300; both from Jackson Immunoresearch) and the Elite ABC kit were applied as above. 3,3′-diaminobenzidine-4HCl (DAB) producing diffuse electron-dense staining was used as a chromogen. The sections were post-fixed with 1% OsO_4, dehydrated, embedded in durcupan (Fluka, Buchs, Switzerland) on microscope slides, and coverslipped. Selected fragments of tissue were analyzed and photographed with an Axioplan 2 microscope (Zeiss, Jena, Germany) and re-embedded into durcupan blocks for electron microscopic investigation. The samples were cut with a Reichert ultramicrotome into 70-nm-thick sections. The sections were then stained with lead citrate and evaluated and photographed in a JEM 1010 electron microscope (JEOL, Japan) equipped with a Multiscan 792 digital camera (Gatan, Pleasanton, CA, USA).

For 3D reconstruction, 20–30 serial images were made with 15,000× magnification of electron microscope. Neuropil fragments were chosen for the 3D reconstruction of axon-like processes in a random manner while avoiding cell bodies and blood vessels when possible. The micrographs were aligned using the computer program Reconstruct [26], publicly available at http://www.bu.edu/neural/Reconstruct.html.

For fluorescent microscopy, NPY-hrGFP mice were perfused with 4% paraformaldehyde and 0.2% picric acid in 0.1 M PB. The brains were removed and immersed overnight in the same fixative. Coronal brain sections (of 50 μm thickness) were cut with a vibratome. For double immunofluorescence staining, the sections were incubated in blocking solution (5% normal goat serum and 0.2% Triton X-100 in 0.1 M PB) for 60 min. The primary polyclonal antibodies (guinea pig anti-CB_1R IgG (CB1-GP-Af530); Frontier Institute, Ishikari, Hokkaido, Japan) and rabbit anti-diacylglycerol lipase-alpha (DAGL) IgG (DGLa-Rb-Af380; Frontier Institute) were both diluted at 1:300 and concomitantly applied overnight at room temperature. The next day, sections were washed 3 times in 0.1 M PB and were concomitantly incubated with the secondary antibodies (goat anti-guinea pig IgG (H+L) Alexa Fluor® 568 conjugate, A-11075; and, goat anti-rabbit IgG (H+L) Alexa Fluor® 633 conjugate; both from Thermo Fischer Scientific, Waltham, MA, USA) both at a dilution of 1:500 for 1 h at room temperature. Finally, the sections were coverslipped in DAKO mounting medium and confocal laser scanning microscopy was performed using a Zeiss LSM Meta 510.

In previous studies, we extensively analyzed specificity of the anti-CB_1R labeling using mass-spectrometry, Western Blots, and immunohistochemistry at light and electron microscopy levels; we demonstrated that anti-CB_1R IgG (CB1-GP-Af530; Frontier Institute) in parallel to CB_1R also recognize a conformational epitope in mitochondrial stomatin-like protein 2 [27–29]. Specific anti-DAGL labeling (neuronal somato-dendritic surface expression) was confirmed for immunohistochemistry at levels of light and electron microscopy using wild type and DAGL-null mice [30–32]. Specific anti-GFP and anti-GFAP labeling was confirmed in numerous studies [e.g., [33,34]].

2.4. Statistical analysis

Quantifications of the anti-CB_1R immunolabeling in identified cell segments and organelles in ARC of the CB_1R-expressing ($CB_1R^{+/+}$ and $CB_1R^{+/-}$, pooled) and $CB_1R^{-/-}$ mice were performed at 15,000× magnification of electron microscope. Percentages of the anti-CB_1R immuno-precipitation locations in axon-like, dendro-somatic, and mitochondrial profiles were calculated for every measurement. Then, averages of 4 measurements from every one of 4 animals in each group ±SD were calculated using Excel 2013 (Microsoft) software.

3. RESULTS

3.1. CB_1R concentrates in axon-like processes in the ARC

Raised in guinea pig anti-CB_1R serum provides intensive staining of CB_1R-expressing cell bodies and axons in the cerebral cortex and hippocampus (Supplementary Figure 1) that is similar to the immunolabeling obtained with other CB_1R antibodies [e.g., [35–37]]. In contrast, anti-CB_1R labeling in the hypothalamus appears as sporadic immunopositive particles that are difficult to distinguish from background staining solely based upon light microscopy or qualitative electron microscopy (Figure 1A–D). Nevertheless, 3D reconstruction from serial sections reveals a dramatic difference in anti-CB_1R labeling

reconstructions are also seen (arrows in **C**). (**D and E**) 3D reconstruction from serial ultrathin sections demonstrates three axons (each depicted with different colors in semi-transparent mode) that contain plural anti-CB_1R DAB-Ni depositions (depicted black; small arrows) and innervate NPY-GFP-negative cells. Red dotted lines indicate positioning of the profiles shown in the electron micrograph in **E** where they are highlighted with the same semitransparent colors, respectively. The yellow synaptic bouton produces symmetric synapse (arrowhead) with the NPY-GFP-negative cell body (semitransparent orange). The green synaptic bouton produces asymmetric synapses (empty arrowheads) with, the NPY-GFP-negative cell body and a dendrite. Several CB_1R-positive axon-like profiles (not shown in 3D) are highlighted semitransparent red. (Scale bars = 1 μm).

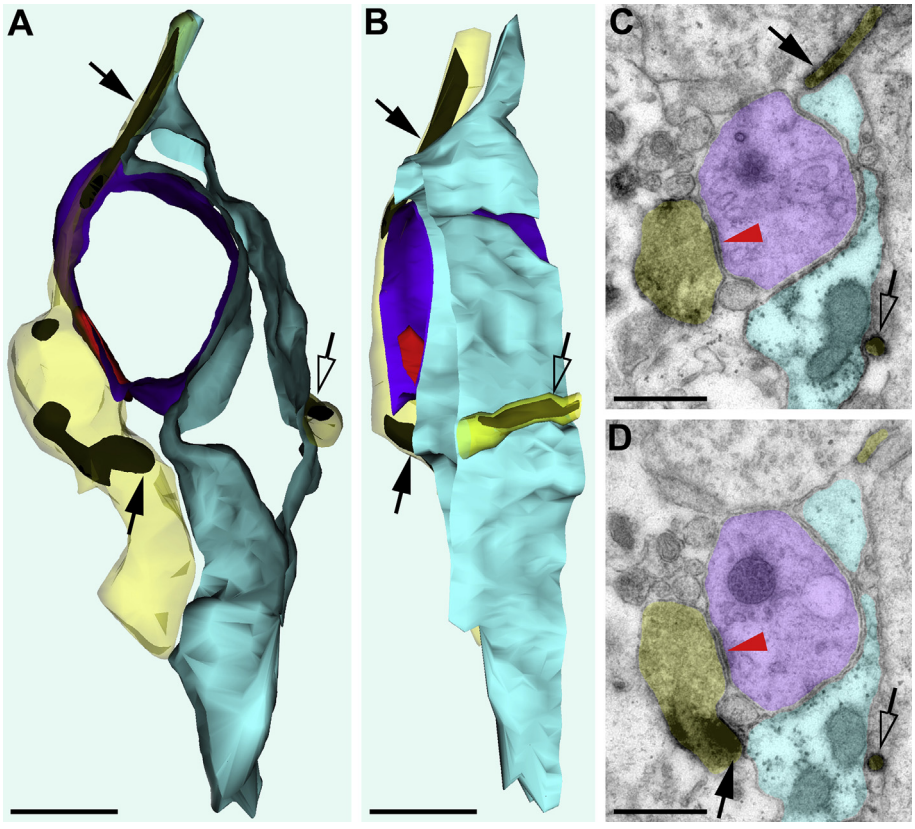

Figure 3: A three-somatic synapse in ARC from $CB_1R^{+/+}$ mouse identified with double immunolabeling for CB_1R (DAB-Ni) and GFAP (DAB) combined with electron microscopy 3D reconstruction. (**A and B**) 3D reconstruction images rotated 90° relative to each other. (**C and D**) Representative serial micrographs used for the 3D reconstruction. CB_1R-containing synaptic bouton (depicted semitransparent yellow in 3D and serial electron micrographs) innervates an immunonegative dendritic shaft (depicted semitransparent indigo). The synaptic contact is shown in red in 3D and indicated with red arrowheads in the electron micrographs. Anti-CB_1R intensive black DAB-Ni depositions (arrows; depicted black in 3D) are seen in both, the synaptic bouton and axonal shafts. Another CB_1R-containing axon-like process (semitransparent yellow; empty arrows) is also seen. Notice that several of the anti-CB_1R DAB-Ni depositions (arrows) contact the GFAP-positive astroglial cell (identified with diffuse DAB staining; highlighted semitransparent light blue), but they are not inside of it. (Scale bars = 0.5 μm).

between CB_1R-expressing and $CB_1R^{-/-}$ animals. We found that each CB_1R-immunopositive process contains several discontinued depositions of anti-CB_1R DAB-Ni immuno-precipitation in the CB_1R wild type ($CB_1R^{+/+}$) and heterozygous ($CB_1R^{+/-}$) mice. In contrast, only a single spot of staining was detected in every 3D-reconstructed process in $CB_1R^{-/-}$ mice, designating occasional binding of the antibodies (Figure 1E, F).

Additional evidence of selective labeling in the CB_1R-expressing animals was obtained with quantification of the sites of DAB-Ni immuno-precipitations in electron microscopy. Analysis of occasional single ultrathin sections shows that 82.2 ± 4.2% of the immuno-precipitations in the CB_1R-expressing mice are located in axon-like processes, whereas the remaining number of immuno-precipitations is distributed between dendrites, cell bodies, and mitochondria (Figure 1G). Predomination of a certain location of anti-CB_1R labeling was not encountered in $CB_1R^{-/-}$ mice. In those, non-CB_1R binding of the CB_1R antibodies (presumed background or labeling of other molecules) was detected in nearly equal proportions in axon-like processes, dendro-somatic cell segments, and mitochondria (Figure 1H). Mind that similar mitochondrial labeling is evident in the CB_1R-expressing and $CB_1R^{-/-}$ mice, confirming previously demonstrated binding of the anti-CB_1R serum with mitochondrial stomatin-like protein 2 rather than revealing mitochondrial location of CB_1R [27–29].

In three random segments of ARC neuropil from $CB_1R^{+/+}$ mice that were subject of electron microscopy analysis and 3D reconstruction (each analyzed volume ~100 μm^3), we identified in total 32, 26, and 13 CB_1R-positive axon-like processes per a reconstructed segment (Supplementary Figure 2). No dendrite-like processes containing CB_1R accumulation were observed in these neuropil segments. Detected CB_1R-positive axon-like processes are separated by immunonegative tissue and do not form CB_1R-enriched bundles that would be easily identifiable with light microscopy. Thus, our quantitative electron microscopy analysis and 3D reconstruction from serial sections demonstrate numerous CB_1R-positive axon-like processes in the hypothalamus.

3.2. CB_1R-expressing axons innervate AgRP/NPY-positive and -negative neurons

To analyze whether the hypothalamic CB_1R-expressing axons could produce synapses innervating AgRP/NPY neurons in the ARC, we performed double immunolabeling for CB_1R and GFP in the NPY-GFP transgenic mice. Using 3D reconstruction from serial sections, we detected CB_1R-positive synapses innervating NPY-GFP-positive dendrites (Figure 2A–C). Among five identified synapses, all were of symmetric morphological type, indicating that inhibitory GABAergic inputs probably predominate among CB_1R-positive synapses that innervate AgRP/NPY neurons. In contrast, NPY-GFP-negative dendritic shafts and cell bodies show both symmetric and asymmetric synaptic contacts with CB_1R-immunopositive axons (Figure 2D, E and Figure 3). Thus, CB_1R-containing synapses innervate AgRP/NPY and other

neurons, supporting the hypothesis for retrograde eCB signaling in the ACR and predomination of eCB-conducted dis-inhibition of the AgRP/NPY hunger promoting neurons. Further morphological study (for example, immuno-gold labeling that provides more precise location of the antigen) of CB_1R location in the hypothalamic nuclei is warranted.

3.3. CB_1R and DAGL are co-localized at AgRP/NPY neurons in ARC

To further elucidate potential CB_1R signaling in ARC, we performed immunofluorescence assay for the enzyme DAGL, which is known to be located at postsynaptic sites catalyzing biosynthesis of the eCB retrograde messenger 2-AG [38,39]. We observed dotted DAGL immunolabeling as in GFP-expressing AgRP/NPY neurons so in GFP-negative cells. Multiple immunofluorescence exemplified a close spatial relationship between CB_1R and DAGL in the ARC, particularly at NPY-GFP neurons (Figure 4). The latter finding supports a retrograde mode of action of 2-AG at AgRP/NPY neurons, as has been demonstrated in other brain segments [5,29].

4. DISCUSSION

Relatively low anti-CB_1R immuno-reactivity in the hypothalamus makes identification of CB_1R-containing axons with light microscopy and in single electron micrographs difficult. Here, we addressed this problem using electron microscopy with 3D reconstruction from serial sections. We show that (1) numerous axons in ARC contain several discontinuous CB_1R-positive segments; (2) CB_1R-positive axons innervate AgRP/NPY neurons with mostly symmetric, presumed inhibitory, synapses; (3) unlabeled neurons receive both symmetric and asymmetric synaptic contacts with CB_1R-positive axons; (4) DAGL — the enzyme catalyzing biosynthesis of the eCB retrograde messenger 2-AG — is in close apposition to CB_1R at AgRP/NPY neurons. Taken together, the data demonstrate the morphologic substrate for eCB/CB_1R-conducted retrograde dis-inhibition of the orexigenic neurons in ARC.

CB_1R and eCBs were shown to be involved in the regulation of food intake and energy consumption in several hypothalamic nuclei, including the lateral and dorsomedial hypothalamus as well as ARC and paraventricular nucleus [1,2,11,13,19,40,41]. Moreover, eCB prandial regulation apparently includes synaptic and non-synaptic mechanisms [10,12,42]. A hypothalamic role of CB_1R-containing synapses in eCB regulation of food intake was suggested [19,22], but it was not experimentally demonstrated. Our findings unravel a yet unknown synaptic mechanism of eCB control of food intake that may act in parallel with recently demonstrated intracellular eCB control of mitochondrial respiration [12].

Thus, our results show that eCBs and cannabis drugs may conduct prandial mechanisms through retrograde synaptic dis-inhibition and dis-excitation in the hypothalamus. Further investigations are warranted to determine the location and neurochemical properties of CB_1R-expressing inhibitory neurons innervating AgRP/NPY neurons in ARC; and, to determine what neurons provide the CB_1R-containing inputs to other neurons of the hypothalamus.

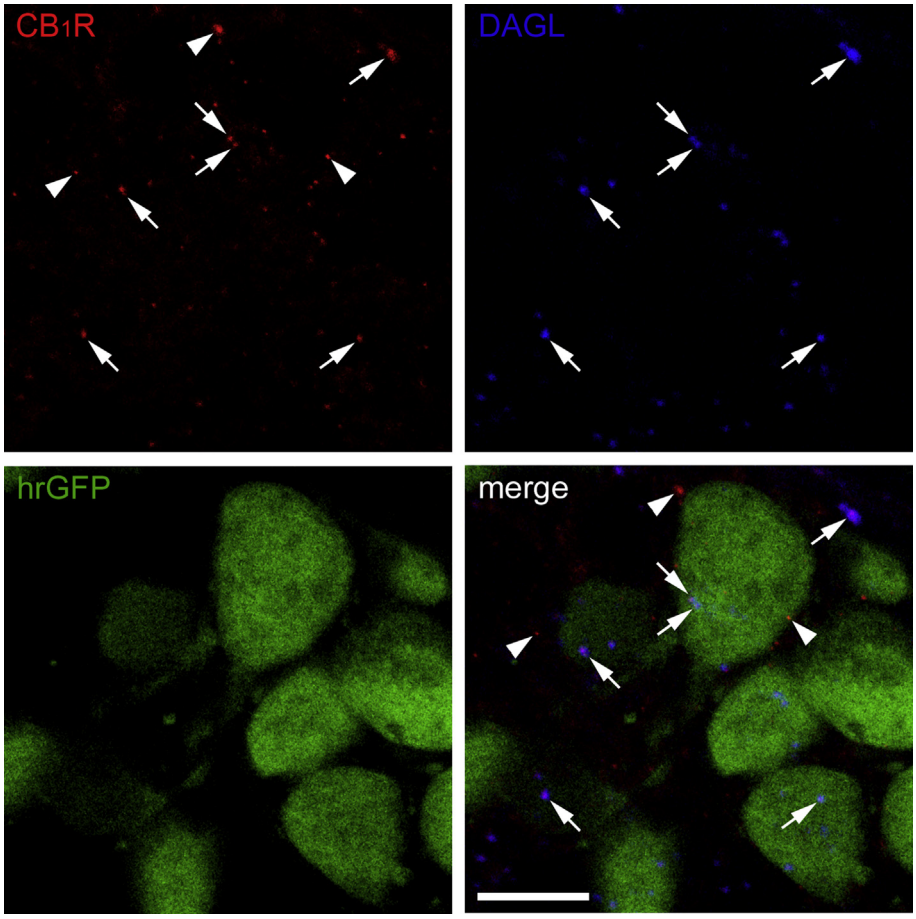

Figure 4: Immunolabeling for CB_1R (red) and DAGL (blue) in ARC from the NPY-hrGFP transgenic mouse. CB_1R/DAGL-double positive spots [some of those are at NPY-hrGFP-expressing cells (green)] are indicated with arrows. CB_1R-positive DAGL-negative spots are indicated with arrowheads. (Scale bar = 10 μm).

AUTHOR CONTRIBUTION

YMM and MK designed and executed experiments, analyzed the data, and wrote the manuscript. TLH and PR analyzed the data and wrote the manuscript.

ACKNOWLEDGMENTS

This work was supported by National Institutes of Health grants AG051459 to TLH; R01DA023999 and R01EY002593 to PR; and by Deutsche Forschungsgemeinschaft SFB 1052/1 (Obesity Mechanisms).

CONFLICT OF INTEREST

All authors declare no conflict of interests.

APPENDIX A. SUPPLEMENTARY DATA

Supplementary data related to this article can be found at http://dx.doi.org/10.1016/j.molmet.2017.01.004.

REFERENCES

[1] DiPatrizio, N.V., Piomelli, D., 2012. The thrifty lipids: endocannabinoids and the neural control of energy conservation. Trends in Neuroscience 35:403–411.

[2] Quarta, C., Bellocchio, L., Mancini, G., Mazza, R., Cervino, C., Braulke, L.J., et al., 2010. CB(1) signaling in forebrain and sympathetic neurons is a key determinant of endocannabinoid actions on energy balance. Cell Metabolism 11:273–285.

[3] Krashes, M.J., Shah, B.P., Madara, J.C., Olson, D.P., Strochlic, D.E., Garfield, A.S., et al., 2014. An excitatory paraventricular nucleus to AgRP neuron circuit that drives hunger. Nature 507(7491):238–242.

[4] Wu, Q., Clark, M.S., Palmiter, R.D., 2012. Deciphering a neuronal circuit that mediates appetite. Nature 483(7391):594–597.

[5] Freund, T.F., Katona, I., Piomelli, D., 2003. Role of endogenous cannabinoids in synaptic signaling. Physiological Reviews 83(3):1017–1066.

[6] Castillo, P.E., Younts, T.J., Chávez, A.E., Hashimotodani, Y., 2012. Endocannabinoid signaling and synaptic function. Neuron 76:70–81.

[7] Di Marzo, V., Goparaju, S.K., Wang, L., Liu, J., Bátkai, S., Járai, Z., et al., 2001. Leptin-regulated endocannabinoids are involved in maintaining food intake. Nature 410:822–825.

[8] Bellocchio, L., Lafenêtre, P., Cannich, A., Cota, D., Puente, N., Grandes, P., et al., 2010. Bimodal control of stimulated food intake by the endocannabinoid system. Nature Neuroscience 13:281–283.

[9] Tam, J., Cinar, R., Liu, J., Godlewski, G., Wesley, D., Jourdan, T., et al., 2012. Peripheral cannabinoid-1 receptor inverse agonism reduces obesity by reversing leptin resistance. Cell Metabolism 16:167–179.

[10] Silvestri, C., Di Marzo, V., 2013. The endocannabinoid system in energy homeostasis and the etiopathology of metabolic disorders. Cell Metabolism 17(4):475–490.

[11] Morello, G., Imperatore, R., Palomba, L., Finelli, C., Labruna, G., Pasanisi, F., et al., 2016. Orexin-A represses satiety-inducing POMC neurons and contributes to obesity via stimulation of endocannabinoid signaling. Proceedings of the National Academy of Sciences of the United States of America 113(17):4759–4764.

[12] Koch, M., Varela, L., Kim, J.G., Kim, J.D., Hernández-Nuño, F., Simonds, S.E., et al., 2015. Hypothalamic POMC neurons promote cannabinoid-induced feeding. Nature 519:45–50.

[13] Cardinal, P., Bellocchio, L., Clark, S., Cannich, A., Klugmann, M., Lutz, B., et al., 2012. Hypothalamic CB1 cannabinoid receptors regulate energy balance in mice. Endocrinology 153(9):4136–4143.

[14] Dietrich, M.O., Liu, Z.W., Horvath, T.L., 2013. Mitochondrial dynamics controlled by mitofusins regulate agrp neuronal activity and diet-induced obesity. Cell 155:188–199.

[15] Dietrich, M.O., Horvath, T.L., 2012. Hypothalamic control of energy balance: insights into the role of synaptic plasticity. Trends in Neuroscience 36:65–73.

[16] Cowley, M.A., Smart, J.L., Rubinstein, M., Cerdán, M.G., Diano, S., Horvath, T.L., et al., 2001. Leptin activates anorexigenic POMC neurons through a neural network in the arcuate nucleus. Nature 411:480–484.

[17] Kola, B., Farkas, I., Christ-Crain, M., Wittmann, G., Lolli, F., Amin, F., et al., 2008. The orexigenic effect of ghrelin is mediated through central activation of the endogenous cannabinoid system. PLoS One 3:e1797.

[18] Kirkham, T.C., Williams, C.M., Fezza, F., Di Marzo, V., 2002. Endocannabinoid levels in rat limbic forebrain and hypothalamus in relation to fasting, feeding and satiation: stimulation of eating by 2-arachidonoyl glycerol. British Journal of Pharmacology 136:550–557.

[19] Cota, D., Marsicano, G., Tschöp, M., Grübler, Y., Flachskamm, C., Schubert, M., et al., 2003. The endogenous cannabinoid system affects energy balance via central orexigenic drive and peripheral lipogenesis. The Journal of Clinical Investigation 112(3):423–431.

[20] Herkenham, M., Lynn, A., Little, M., Johnson, M., Melvin, L., Costa, B.D., et al., 1990. Cannabinoid receptor localization in brain. Proceedings of the National Academy of Sciences of the United States of America 87:1932–1936.

[21] Matsuda, L., Lolait, S., Brownstein, M., Young, A., Bonner, T., 1990. Structure of a cannabinoid receptor and functional expression of the cloned cDNA. Nature 346:561–564.

[22] Horvath, T.L., 2003. Endocannabinoids and the regulation of body fat: the smoke is clearing. The Journal of Clinical Investigation 112:323–326.

[23] Bermudez-Silva, F.J., Cardinal, P., Cota, D., 2012. The role of the endocannabinoid system in the neuroendocrine regulation of energy balance. Journal of Psychopharmacology 26:114–124.

[24] Wittmann, G., Deli, L., Kalló, I., Hrabovszky, E., Watanabe, M., Liposits, Z., et al., 2007. Distribution of type 1 cannabinoid receptor (CB1)-immunoreactive axons in the mouse hypothalamus. The Journal of Comparative Neurology 503(2):270–279.

[25] Zimmer, A., Zimmer, A.M., Hohmann, A.G., Herkenham, M., Bonner, T.I., 1999. Increased mortality, hypoactivity, and hypoalgesia in cannabinoid CB_1 receptor knockout mice. Proceedings of the National Academy of Sciences of the United States of America 96:5780–5785.

[26] Fiala, J.C., Harris, K.M., 2001. Extending unbiased stereology of brain ultrastructure to three-dimensional volumes. Journal of the American Medical Informatics Association 8(1):1–16.

[27] Morozov, Y.M., Dominguez, M.H., Varela, L., Shanabrough, M., Koch, M., Horvath, T.L., et al., 2013. Antibodies to cannabinoid type 1 receptor co-react with stomatin-like protein 2 in mouse brain mitochondria. The European Journal of Neuroscience 38:2341–2348.

[28] Morozov, Y.M., Horvath, T.L., Rakic, P., 2014. A tale of two methods: identifying neuronal CB1 receptors. Molecular Metabolism 3(4):338.

[29] Morozov, Y.M., Sun, Y.-Y., Kuan, C.-Y., Rakic, P., 2016. Alteration of SLP2-like immunolabeling in mitochondria signifies early cellular damage in developing and adult mouse brain. The European Journal of Neuroscience 43:245–257.

[30] Yoshida, T., Fukaya, M., Uchigashima, M., Miura, E., Kamiya, H., Kano, M., et al., 2006. Localization of diacylglycerol lipase-alpha around postsynaptic spine suggests close proximity between production site of an endocannabinoid, 2-arachidonoyl-glycerol, and presynaptic cannabinoid CB1 receptor. The Journal of Neuroscience 26(18):4740–4751.

[31] Uchigashima, M., Narushima, M., Fukaya, M., Katona, I., Kano, M., Watanabe, M., 2007. Subcellular arrangement of molecules for 2-arachidonoyl-glycerol-mediated retrograde signaling and its physiological contribution to synaptic modulation in the striatum. The Journal of Neuroscience 27(14):3663–3676.

[32] Reguero, L., Puente, N., Elezgarai, I., Ramos-Uriarte, A., Gerrikagoitia, I., Bueno-López, J.L., et al., 2014. Subcellular localization of NAPE-PLD and

DAGL-α in the ventromedial nucleus of the hypothalamus by a preembedding immunogold method. Histochemistry and Cell Biology 141(5):543—550.

[33] Lee, M.M., Arrenberg, A.B., Aksay, E.R., 2015. A structural and genotypic scaffold underlying temporal integration. The Journal of Neuroscience 35(20): 7903—7920.

[34] O'Brien, E.E., Smeester, B.A., Michlitsch, K.S., Lee, J.H., Beitz, A.J., 2015. Colocalization of aromatase in spinal cord astrocytes: differences in expression and relationship to mechanical and thermal hyperalgesia in murine models of a painful and a non-painful bone tumor. Neuroscience 301:235—245.

[35] Morozov, Y.M., Freund, T.F., 2003. Post-natal development of type 1 cannabinoid receptor immunoreactivity in the rat hippocampus. The European Journal of Neuroscience 18:1213—1222.

[36] Bodor, A.L., Katona, I., Nyíri, G., Mackie, K., Ledent, C., Hájos, N., et al., 2005. Endocannabinoid signaling in rat somatosensory cortex: laminar differences and involvement of specific interneuron types. The Journal of Neuroscience 25(29):6845—6856.

[37] Katona, I., Sperlágh, B., Sík, A., Käfalvi, A., Vizi, E.S., Mackie, K., et al., 1999. Presynaptically located CB1 cannabinoid receptors regulate GABA release from axon terminals of specific hippocampal interneurons. The Journal of Neuroscience 19:4544—4558.

[38] Katona, I., Urban, G.M., Wallace, M., Ledent, C., Jung, K.M., Piomelli, D., et al., 2006. Molecular composition of the endocannabinoid system at glutamatergic synapses. The Journal of Neuroscience 26:5628—5637.

[39] Ohno-Shosaku, T., Maejima, T., Kano, M., 2001. Endogenous cannabinoids mediate retrograde signals from depolarized postsynaptic neurons to presynaptic terminals. Neuron 29:729—738.

[40] Pagotto, U., Marsicano, G., Cota, D., Lutz, B., Pasquali, R., 2006. The emerging role of the endocannabinoid system in endocrine regulation and energy balance. Endocrine Reviews 27(1):73—100.

[41] Hentges, S.T., Low, M.J., Williams, J.T., 2005. Differential regulation of synaptic inputs by constitutively released endocannabinoids and exogenous cannabinoids. Journal of Neuroscience 25:9746—9751.

[42] Bosier, B., Bellocchio, L., Metna-Laurent, M., Soria-Gomez, E., Matias, I., Hebert-Chatelain, E., et al., 2013. Astroglial CB1 cannabinoid receptors regulate leptin signaling in mouse brain astrocytes. Molecular Metabolism 2(4): 393—404.

